Chapter 6. Model comparison

6.1 comparison with RQMD

Data shown in the previous chapter are compared with a microscopic cascade model 'relativistic quantum molecular dynamics' (RQMD). The characteristics of the RQMD model will be pointed. (1) The interaction probabilities are given by geometry. (2) The dominant production mechanism in the first stage of the collision is the excitation of both collision partners to resonances or strings. (3) Excitation of baryons can also be come from the secondary interactions, which are dominated by annihilation of produced mesons on baryons. (4) Those formed resonances contribute to strangeness enrichment and are further excited by subsequent collisions to create $N\overline{N}$. (5) The formation time of newly produced secondaries is given by the finite life time of a resonance or by the time which a string needs to break into parts which is given by the momenta of the fragments. (6) Such multistep process is viewed as a complicated interplay between excitation and decay processes. (7) The fate of all particles including newly produced ones as well as the original ones is followed by propagating those particles on classical trajectories and allowing collisions between all of them until the cascade process is finished.

Transverse mass spectra for three particle species for both colliding systems are compared with the RQMD model, too. The figure 6-1 shown here is the same one in the previous chapter, and RQMD spectra are overlapped for each slopes. The invariant cross sections $1/M_T\ dN/dM_T$ are arbitrary normalized for each spectra. The transverse mass spectra calculated by the RQMD model agree with the inverse slopes for pions, kaons and protons for both sulphur on sulphur collision system and lead on lead collision seen in the experimental data, except low P_T pions for both systems and low P_T protons for Pb+Pb collisions. Global trends of the slopes for those three particles are reproduced by the microscopic cascade RQMD model. This suggests that the transverse flow effect which has been described in the previous chapter might be created by superimposing of binary N+N collisions and re-scattering cascade during the collisions.

Comparison of measured transverse mass spectra by NA44 and NA35 and one from RQMD simulation for pion for S+S and Pb+Pb collisions is shown in the figure 6-2, where one can see clear deviation between experimental measurement and RQMD simulation at low P_T region. Heavy or long lived resonances contributions to the pion M_T spectra from RQMD simulation are shown in the figure 6-3. Those resonances contributions are clearly seen at lower P_T region and make the steep component, which corresponds to the small inverse slope parameter, in the invariant M_T distribution. Low P_T enhancement can be explained with those contributions qualitatively, but quantitatively the low P_T enhancement is not enough in the RQMD simulation, although the data from both NA44 and NA35 experiment [5-2] show more remarkable enhancement, which can be found in the figure 6-2. The heavy or long lived resonances contributions have also studied for the emission position

distribution of the secondary hadrons as seen in the figure 6-4. Those resonances contributions are found to be wider than the others seen in the figure, because of the longer life time. Combining two pictures of transverse mass spectra and emission position distributions with or without the resonances contributions, those resonances will affect the pion transverse mass spectrum at lower P_T region, which will cause the low P_T enhancement, and the large pion source size at low P_T region. This tendencies are consistent with the experimental measurements, qualitatively.

Proton rapidity distribution are compared between RQMD model and data measured at NA44 experiment shown in the figure 6-5. Similar centrality selection to RQMD events is done to compare it with the experimental data. For comparison, RQMD calculation for proton on proton collision is added on the top of the figure in order to compare with sulphur on sulphur collisions and lead on lead collisions. Integrated number of the proton rapidity distribution should be conserved to almost the number of the original colliding two nuclei as mentioned in the previous chapter. The fraction of the number of the stopped protons at the central rapidity region is clearly increasing with the size of the colliding system. Higher degree of the nuclear stopping power is also seen in the RQMD model at truly heavy-ion collisions. The value and shape of dN/dy of RQMD model reproduce the experimental data fairly well. Rapidity shifts, which correspond to a direct measurement of the nuclear stopping power, are calculated as an average rapidity over the forward rapidity region except the spectator peak at the rapidity wing, by using the dN/dy distribution of RQMD simulation. Those numbers are seen in the figures, and are the highest almost around 2 units of rapidity at the heaviest lead on lead collisions. This also proves the higher stopping power at the heaviest system at SPS energy.

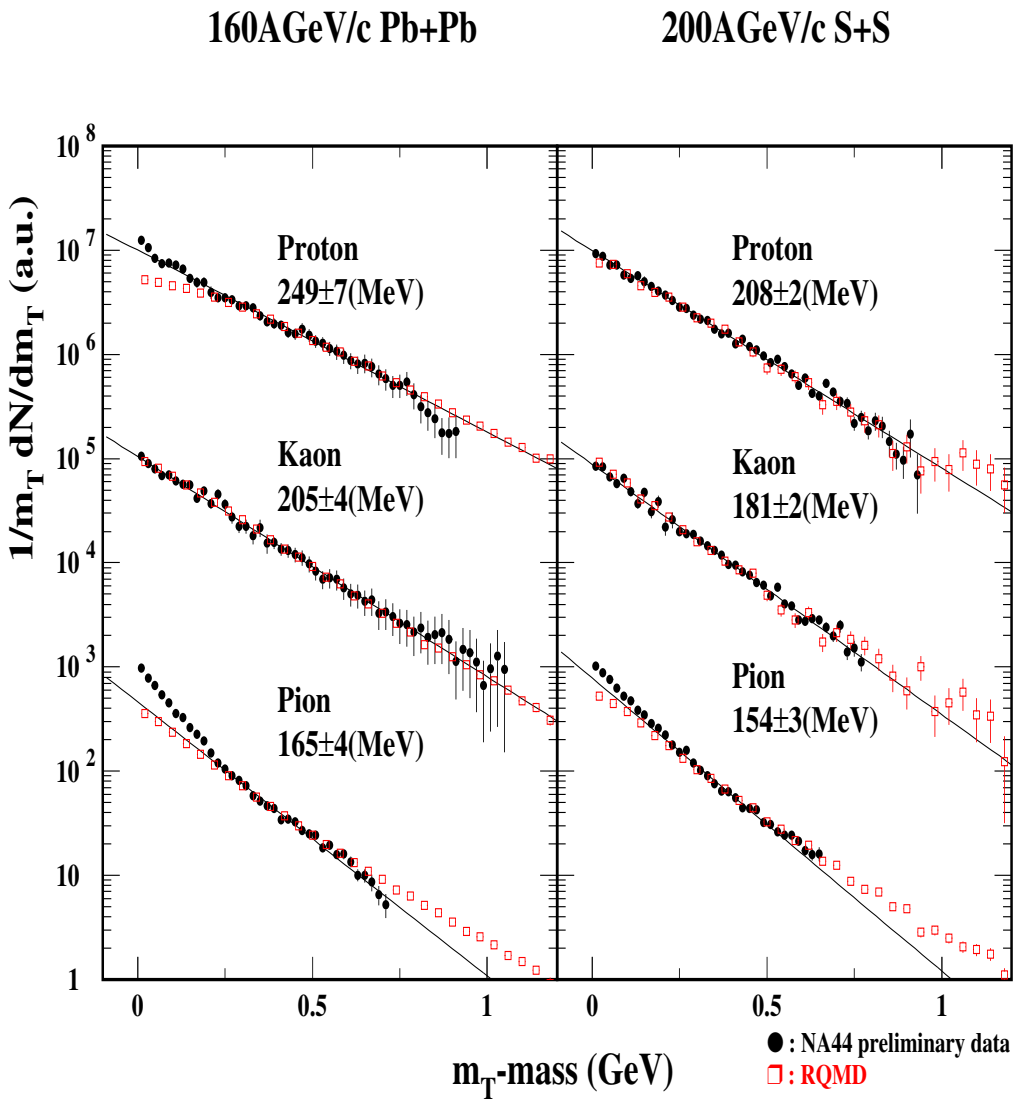

Figure 6-1: transverse mass spectra

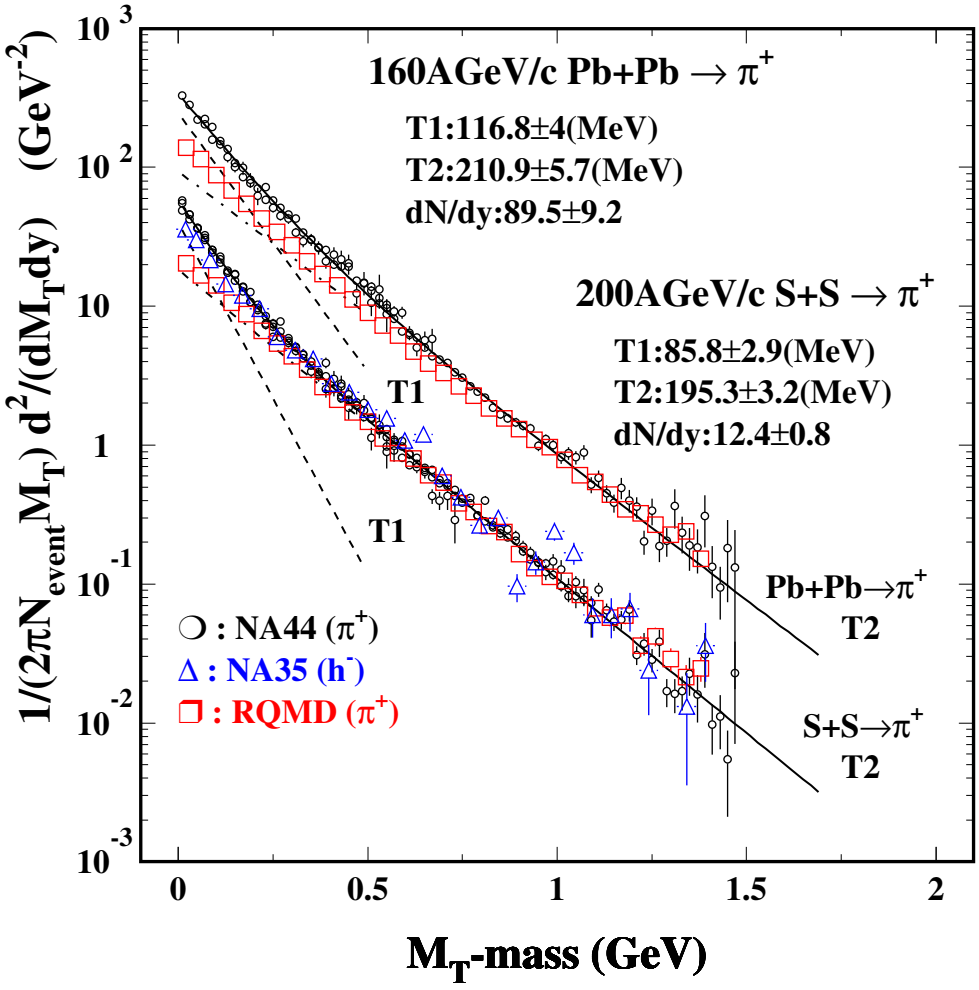

Figure 6-2: comparison of inverse slopes for pion

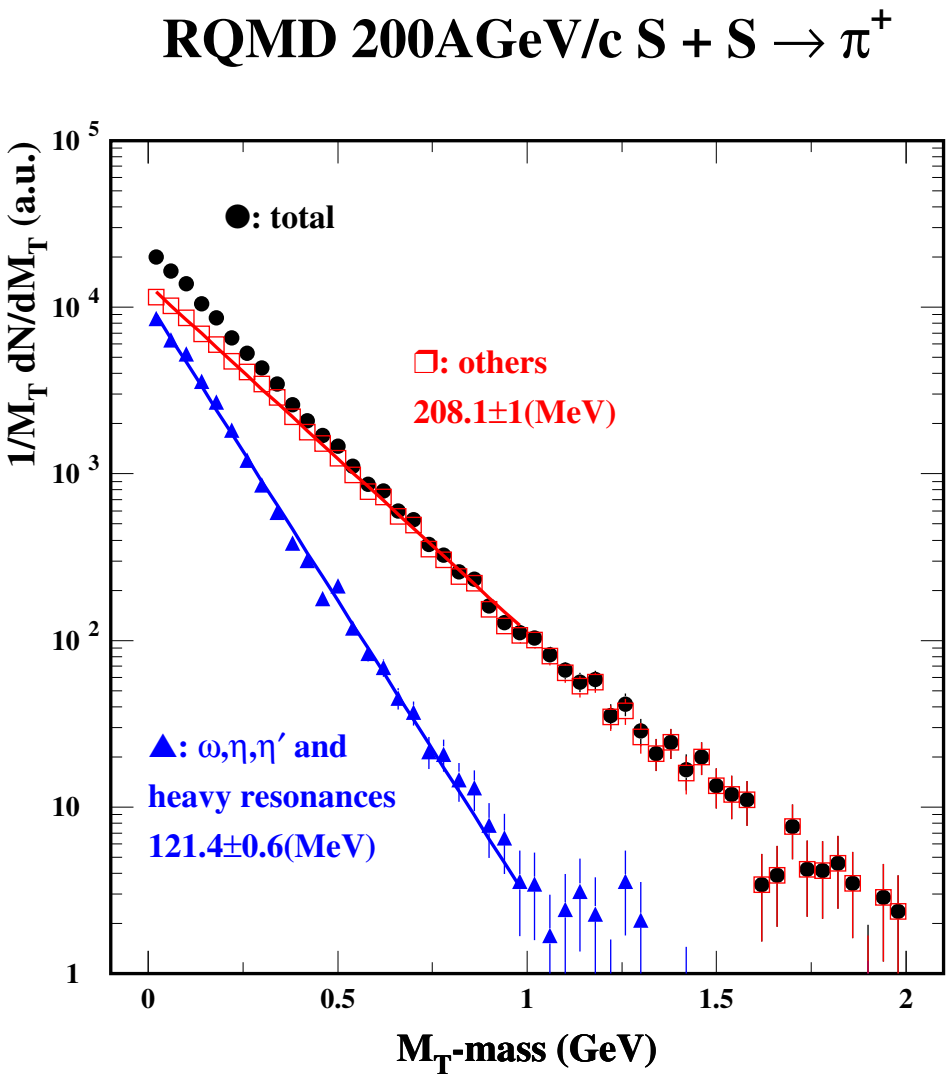

Figure 6-3: heavy resonance contribution to inverse slope

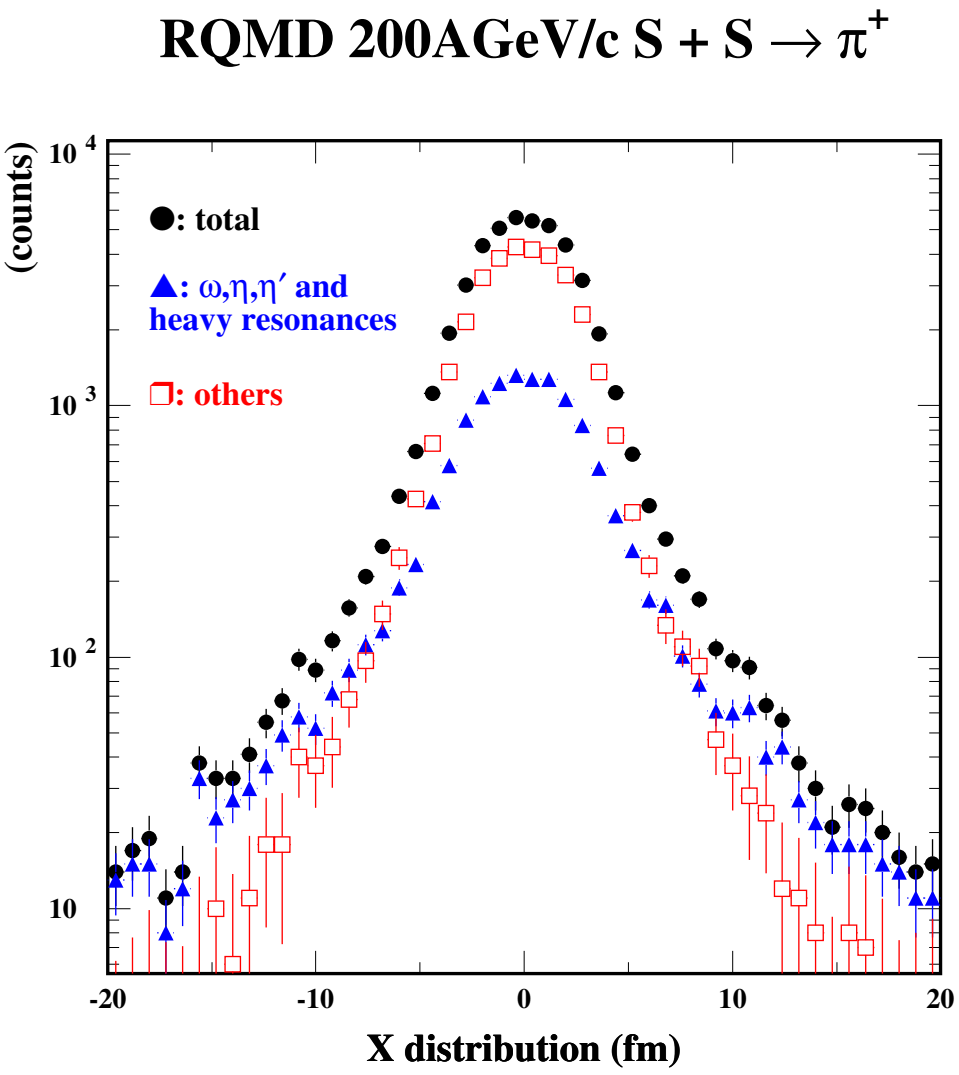

Figure 6-4: heavy resonance contribution to source distribution

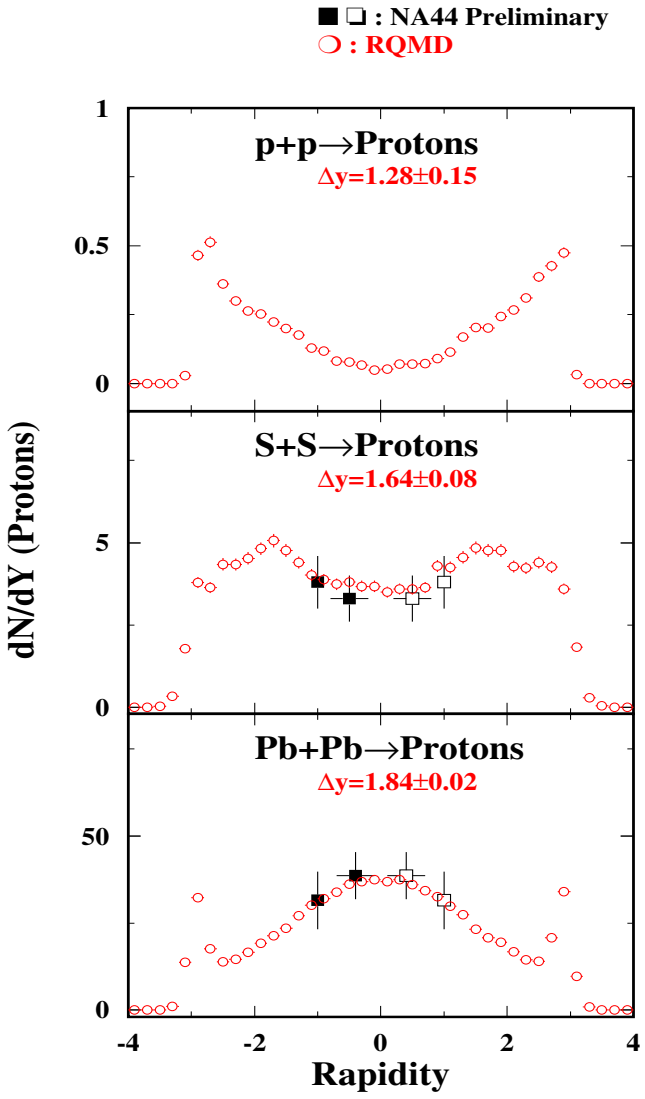

Figure 6-5: proton dN/dy distributions

Pion source distributions from the RQMD simulation are made for each slices of P_T range shown in the figure 6-6. As one can see that the width of the whole distribution does not change with increasing the P_T too much. However, inspecting the center-top shape of each distribution, rather flat bell shape distribution at lower P_T region is changed to volcanic U shape distribution, which will make the doughnut shape in X-Y plane, at higher P_T. This change is caused by the previous mentioned position-momentum correlation of the expanding source. Superimposed histograms are accepted-particle source distributions by the NA44 spectrometer at 4GeV/c small angle, 4GeV/c large angle and 8GeV/c large angle settings. The accepted-particle distribution changes its own peak position toward the negative X direction and the width of the distribution decreases with increasing the P_T, this is purely kinematical effect, that is the position-momentum correlation and the experimental acceptance. X distributions requiring the acceptance are always shifted toward negative in X direction, the reason of this is that (1) the NA44 spectrometer is sitting at the negative X side respecting to the beam line, and (2) therefore the experimental momentum acceptance covers mainly negative P_X ($-0.4 < P_X < 0.05$ GeV/c for 4GeV/c small angle setting, $-0.8 < P_X < -0.2$ GeV/c for 4GeV/c large angle setting and $-0.6 < P_X < 0.05$ GeV/c for 6GeV/c small angle setting), although P_Y acceptance is symmetry and small ($\pm$ 0.05 GeV/c), and (3) strong position-momentum correlation of expanding source distribution, which is demonstrated with the RQMD simulation in the figure 6-7. Experimental acceptance itself has a tendency to reduce the size of particle emitting source distribution with increasing P_T. The figure 6-8 summarizes the width of the pion source distribution with and without requiring the experimental acceptance as a function of M_T.

Source distributions of pion and kaon given by the RQMD simulation are shown in the figure 6-9. Top two figures show the pion source distributions in X and Y directions, where both directions are perpendicular to the beam direction, bottom two figures are same for kaon source distributions. Kaon source is found to be smaller than pion without requiring experimental acceptance. Several reasons can be listed, kaons are less affected by resonance decay than pions, the smaller cross section of kaon with nuclear matter compared to pion may cause the different (earlier) decoupling time from the particle emitting source. Superimposed histograms in the same figure show the same source distributions with requiring the acceptance for pion at 4GeV/c small angle setting corresponding to low P_T region and at 4GeV/c large angle setting corresponding to high P_T region, and for kaon at 6GeV/c small angle setting. The next figure 6-10 also shows the emission source distributions (X, Y, Z, and time) in the LCMS frame, where total P_Z of two particles is zero, which can be defined only with two particle events in the experimental acceptance. The fitted sigma parameter with Gaussian function are shown in the figures for each distribution. A trend of experimentally measured radius parameters for various settings with the interferometry technique are reproduced qualitatively in the RQMD emission source distributions. This may suggest that the source length scale of particle emitting source distribution with requiring the NA44 experimental acceptance is smaller than the length scale created by the position-momentum correlation from

the expansion.

By using RQMD source distribution cooperated with SPACER program, correlation functions are created to compare the shape of the correlation functions and to compare measured source size by fitting the correlation function with the experimental data. The spacer program calculates a correlation function for given single particle phase-space distribution by symmetrizing the wave function, therefore in this way, the fitted source size parameter will be affected by the position-momentum correlation generated in the RQMD simulation. Created correlation functions are compared with experimental correlation functions for each setting, the comparison is shown in the figure 6-11. Correlation functions without resonance, (no ω, η, η' for pion), (no ϕ, K^* for kaon) are superimposed on those figures in order to see the effect of the resonances. Those resonances contribute to make the λ parameter smaller, where the λ shows an amplitude of the correlation and is intersection of the correlation function, and to make the width of the enhancement smaller, which means that it makes the radius parameter larger. Those effects are found to be larger at low P_T as seen in the single particle spectrum. Fitted radius parameters from this calculation have a similar trend found in the experimental data, although the λ parameters of the calculation are larger than that of experimental data for all cases. This also tells that the resonances contribution in RQMD simulation is not enough compared with the experimental data. The source distribution and the correlation function of pion at 8GeV/c large angle setting are also calculated with the simulation, although there is no experimental data. The width of the fitted source distribution ($\sigma_{\rm dist}$) from RQMD simulation and the fitted source size of the correlation function created by RQMD simulation and SPACER program are shown to compare with the measured source size in the figure 6-12. The simulation shows a clear deviation in R_T from the fitted function $1/\sqrt{M_T}$ to the experimental data. The experimental data measured at 8GeV/c large angle setting will give clear and unique solution.

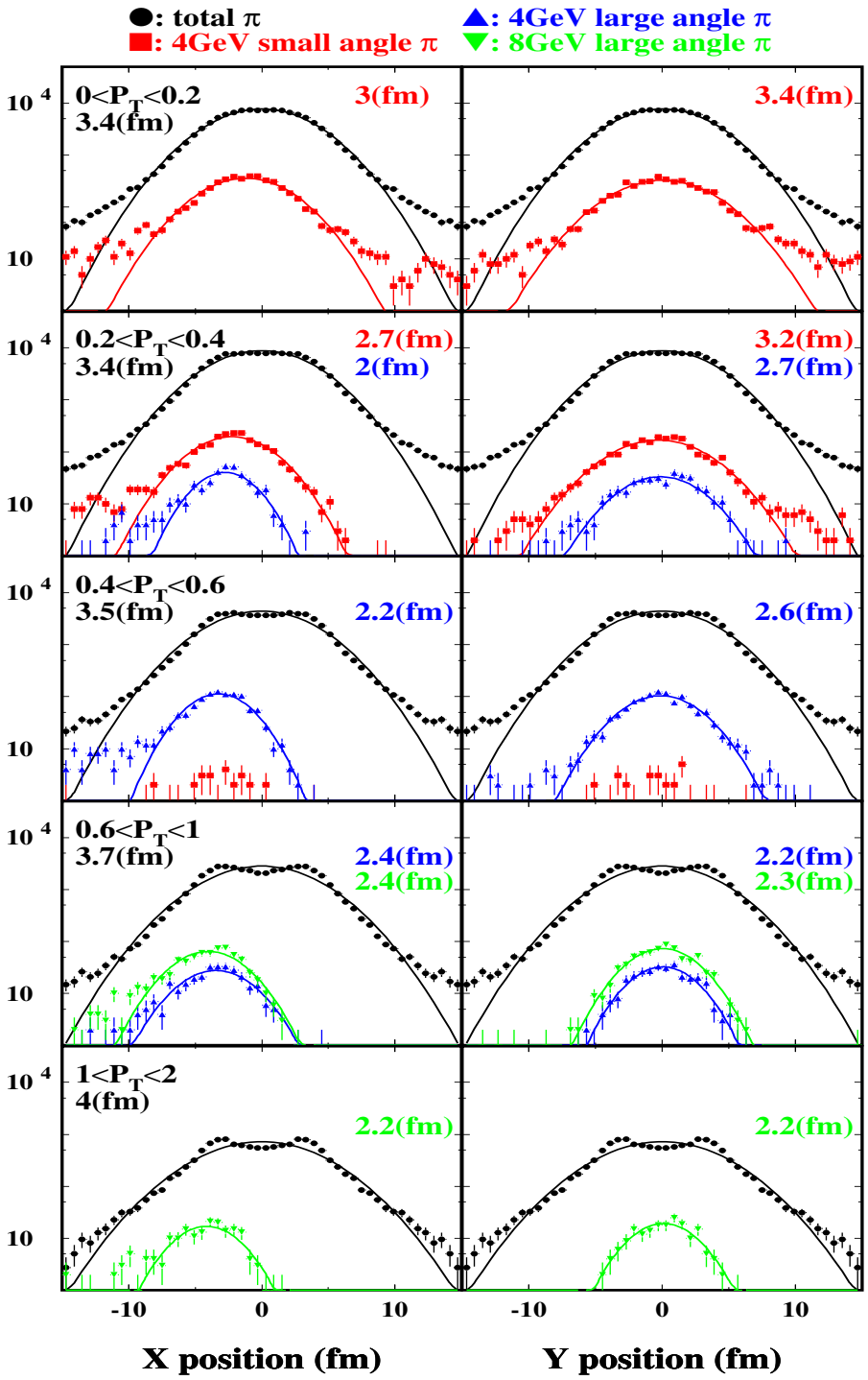

Figure 6-6: P_T dependence of the pion source distribution

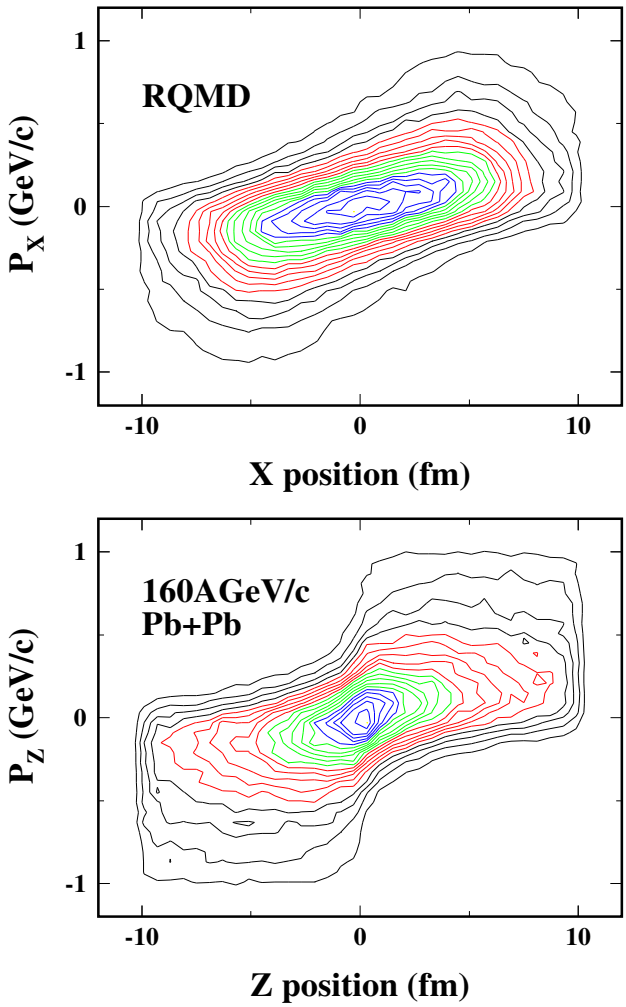

Figure 6-7: position-momentum correlation generated in RQMD

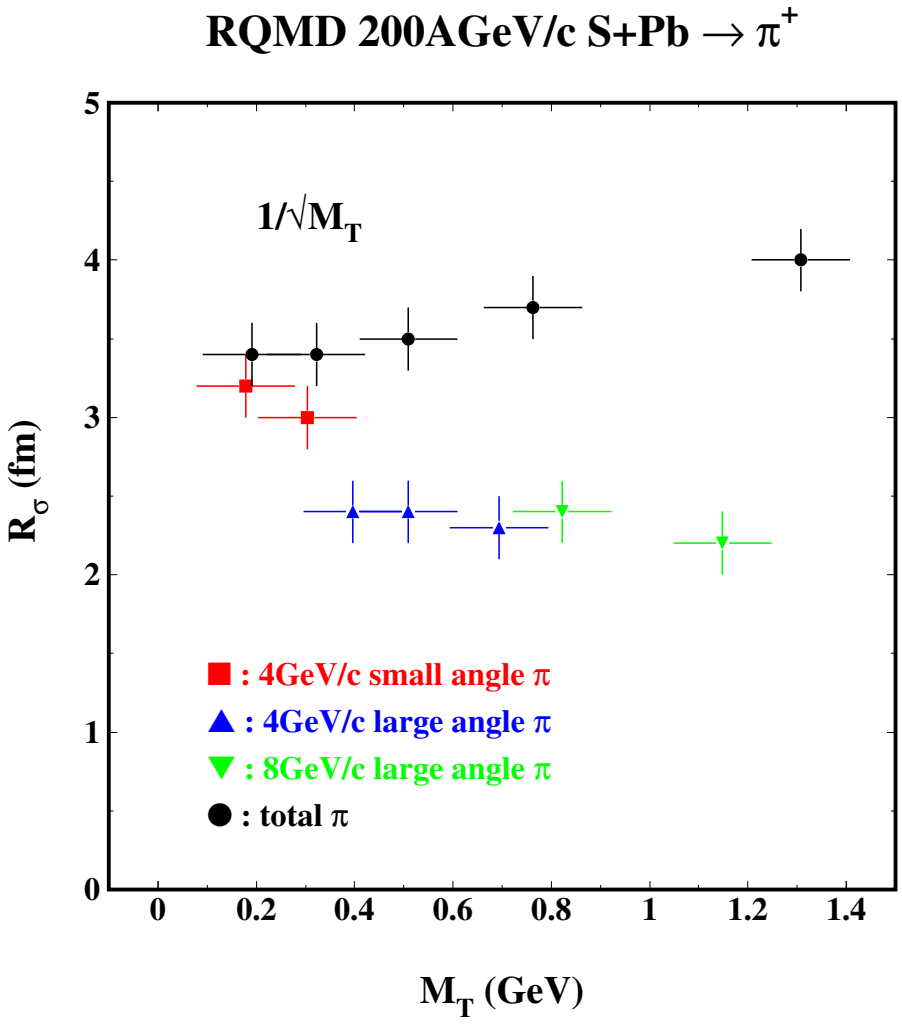

Figure 6-8: summary of the width of the pion source distribution

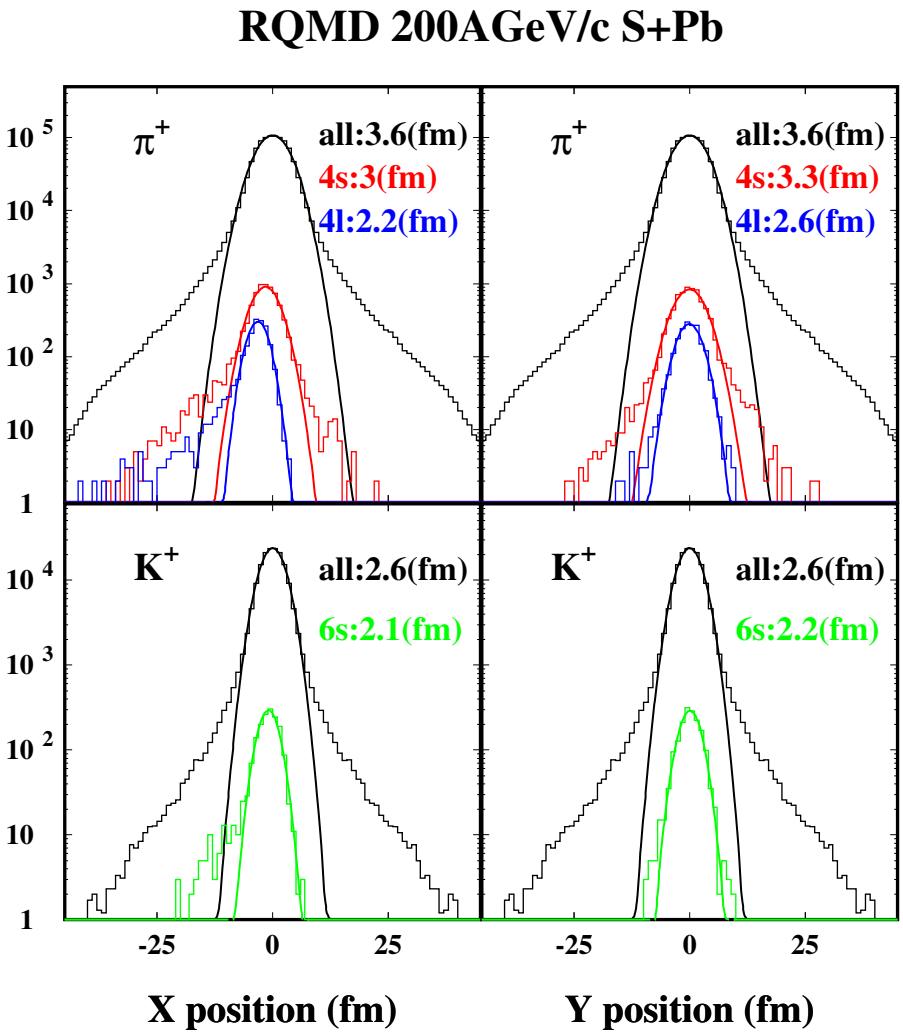

Figure 6-9: source distributions for pion and kaon

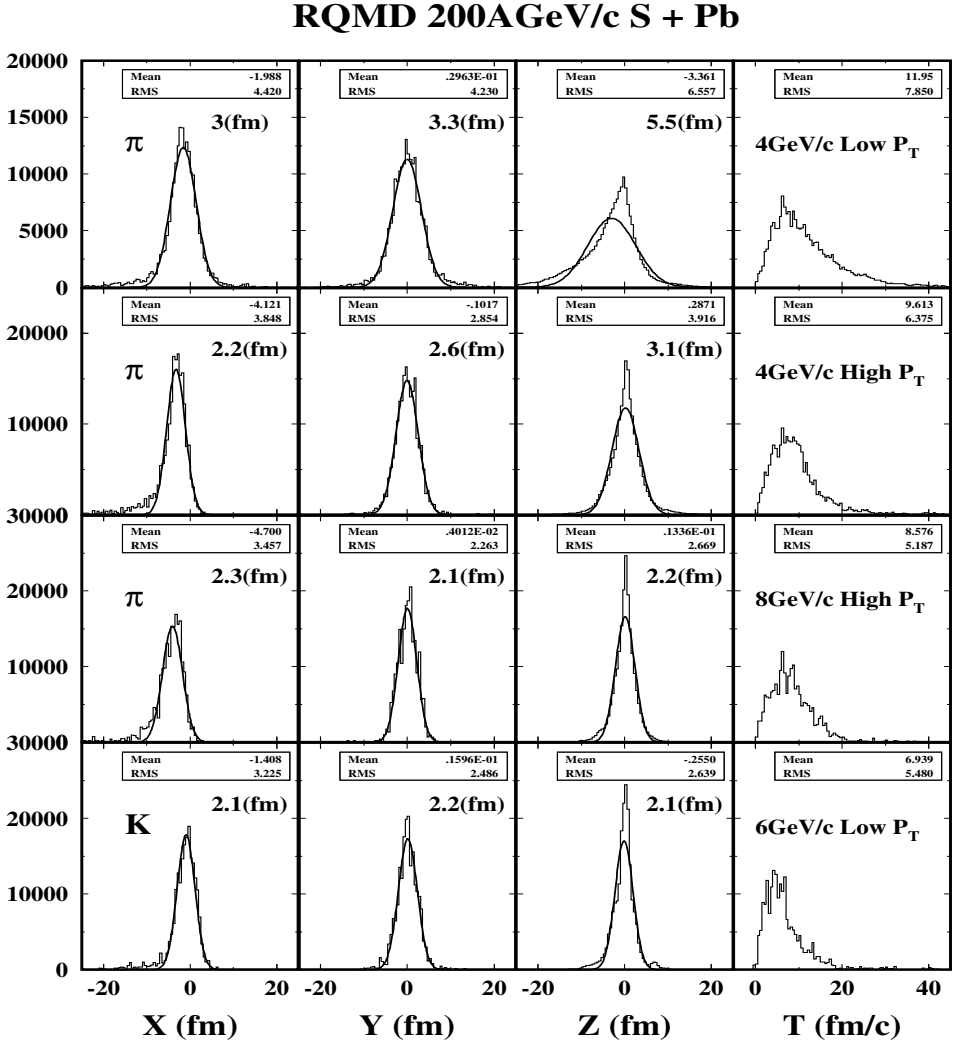

Figure 6-10: source distributions for several settings

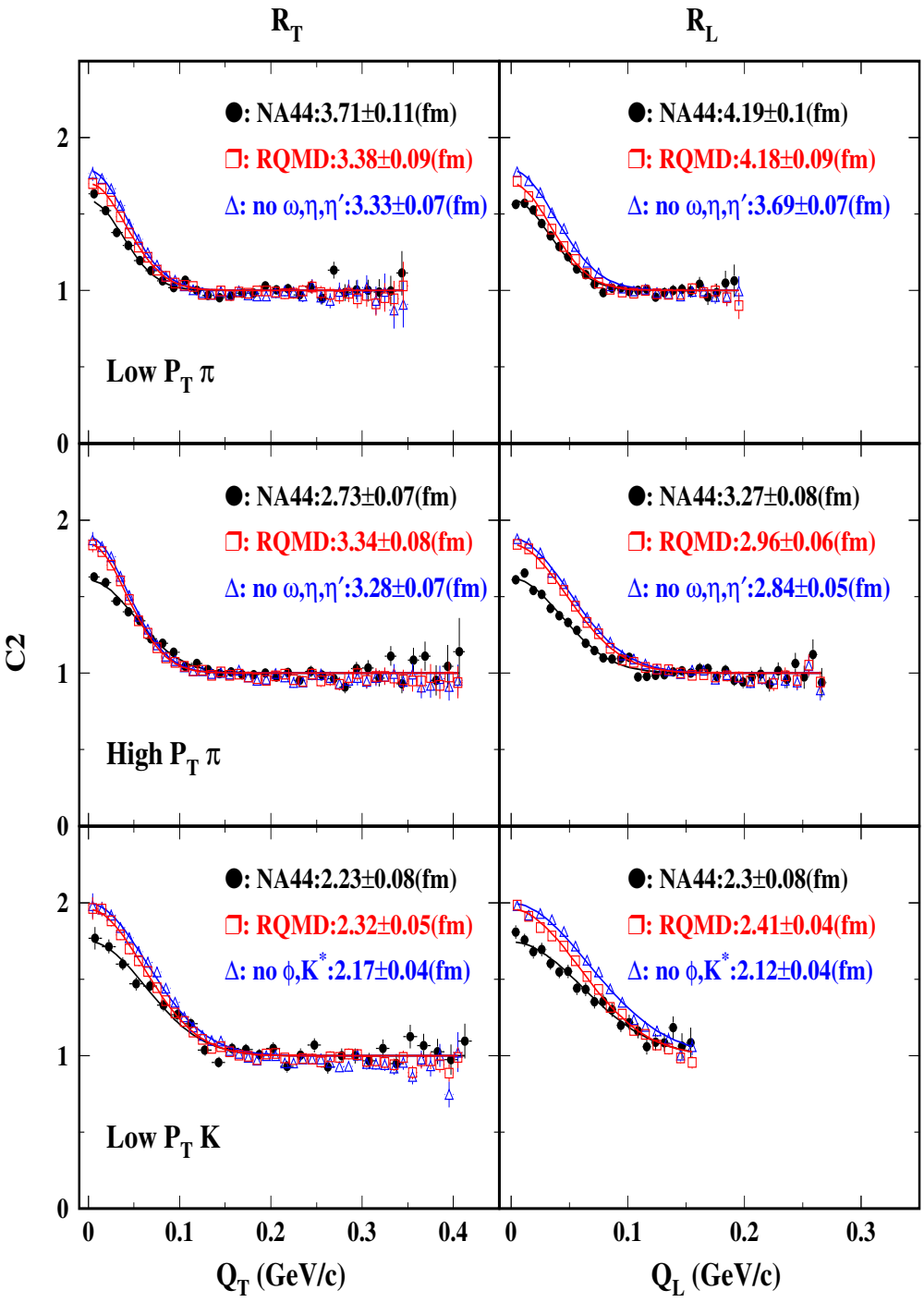

Figure 6-11: comparison of correlation functions

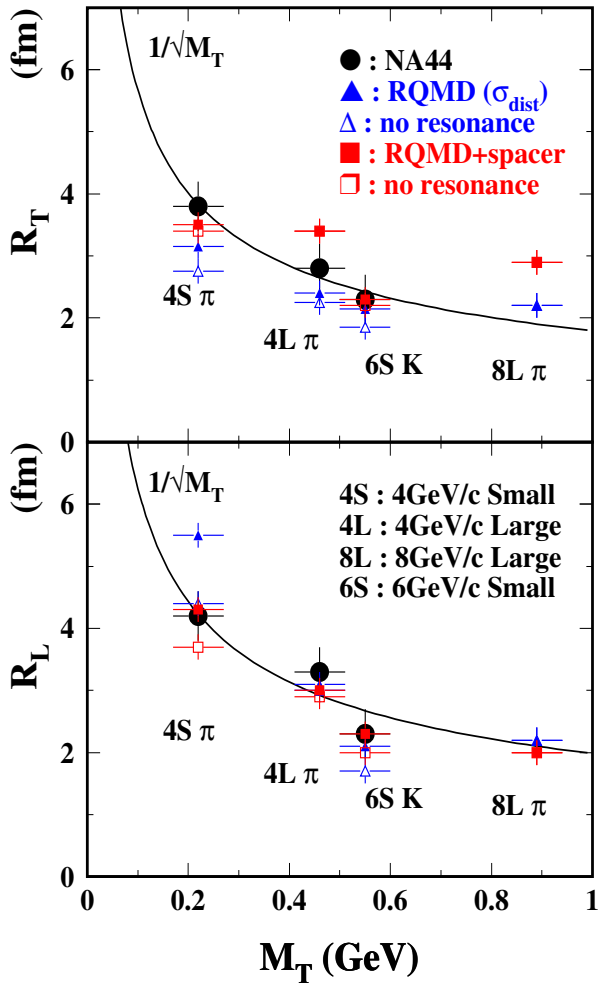

Figure 6-12: summary of the source size

6.2 comparison with hydro-dynamical model calculation

The transverse mass spectra are compared with a hydro-dynamical model calculation. The formula of transverse mass spectrum from the hydro-dynamical model calculation can be found in the reference and is described in the following formula.

$$\frac{1}{M_T}\frac{dN}{dM_T} \propto \int_0^R r dr M_T I_0(\frac{P_T sinh\rho}{T_f}) K_1(\frac{M_T cosh\rho}{T_f}),$$

where the spectrum is a superposition of the individual thermal components, which are boosted with the boost angle $\rho = tanh^{-1}\beta(r)$. $\beta(r)$ is a transverse velocity distribution, which is defined as $\beta(r) = \beta_s(r/R)^\alpha$ in the region of $(0 < r < R)$, where a power of α will change the form of the velocity profile. In the following calculation, $\alpha = 1$ is used. I_0 and K_1 are well known as modified bessel functions. This formula is therefore parameterized by a freeze-out temperature (T_f), a surface velocity (β_s) and a mass of the particle [6-2,3].

Now, this transverse mass spectrum given by the formula is used to describe the experimentally measured spectrums shown in the previous chapter. Three experimentally measured slopes of pions, kaons and protons for each colliding system will be tried to be reproduced by the hydro-dynamical calculation with single T_f and β_s, in order to examine a scenario that an expanding fire ball of the colliding system will be frozen-out (hadronized) at a constant freeze-out temperature T_f for all hadrons with a maximum surface velocity β_s. By fitting those three slopes at a same time, the resulting fitted parameters of T_f and β_s will be given for both S+S and Pb+Pb colliding systems, this will give us some informations for understanding the difference of the expansion or freeze-out feature between the two colliding systems. One set of parameters T_f and β_s successively reproduces the invariant cross sections of pions, kaons and protons as a function of $M_T - mass$ for both sulphur on sulphur collisions and lead on lead collisions, as seen in the figure 6-13, the calculated points are shown in open squares for each slopes. In this calculation, the same freeze-out temperature ($T_f = 140$ MeV) for both colliding systems as a pion mass and is also Hagedorn limit and the different surface velocity ($\beta_s = 0.4$ for S+S and $\beta_s = 0.5$ for Pb+Pb) are used. The figures 6-14 and 6-15 show the comparison between this hydro-dynamical model and the experimental data at the different freeze-out temperature, $T_f = 120$ MeV and $T_f = 100$ MeV, respectively. The model calculations reproduce the measured M_T spectra fairly well for each case.

After making the three slopes for pion, kaon and proton with the above explained formula using the different mass for each particle by fixing the T_f and β_s, one normalization parameter will be fitted for each particle to minimize the fitted chi-square value. Then the total chi-square will be added for those three slopes with the fixed T_f and β_s. This total chi-square will be calculated over and over again in every steps of the T_f and β_s in order to make chi-square map over the two dimensional parameter space of the T_f and β_s. This calculations are done for both colliding systems separately, chi-square contour maps for both systems are shown in the figure

6-16. By looking at the each chi-square map, the resulting parameters T_f and β_s are seen to be not unique, minimum chi-square region has strong correlation between T_f and β_s around (100 MeV $< T_f <$ 140 MeV for both cases, $0.4 < \beta_s < 0.6$ for S+S and $0.5 < \beta_s < 0.7$ for Pb+Pb). However, at any fixed freeze-out temperature T_f, an increase of the surface velocity β_s from lighter to heavier system is clearly seen from those two chi-square contour maps. This also suggests an increase of the transverse flow in truly heavy-ion collision at SPS energy compared to the lighter heavy-ion systems.

Velocity profile dependence of the chi-square contour map is studied by changing the power of α to be 0.5, 1.0 and 2.0. To compare the shape effect with the velocity profile from $\beta(r) = \beta_s(r/R)^\alpha$, the velocity profile from RQMD simulation is extracted by fitting the RQMD profile distribution with the following sigmoid function.

$$\beta(r) = \frac{\beta_s}{exp\{-B\ (r - A)\} + 1},$$

where A and B are the fitting parameters to the profile distribution. Comparison of the velocity profiles is shown in the figure 6-17. By using the four different profiles α = 0.5, 1.0, 2.0 and RQMD type, chi-square contour maps are created over 2-dimensional space T_f and β_s for each velocity profile and for each colliding system. Figure 6-18 shows the chi-square contour maps for different velocity profiles. The resulting T_f and β_s having a minimum chi-square are found to be sensitive to the velocity profile and RQMD profile is somehow similar to α=0.5 velocity profile. α parameter seems to be correlated with β_s, although it does not affect to T_f too much, which might remind one of the roll of the constant C in the formula $T_m = T_f + C\beta_s^2 M$ shown in the previous chapter.

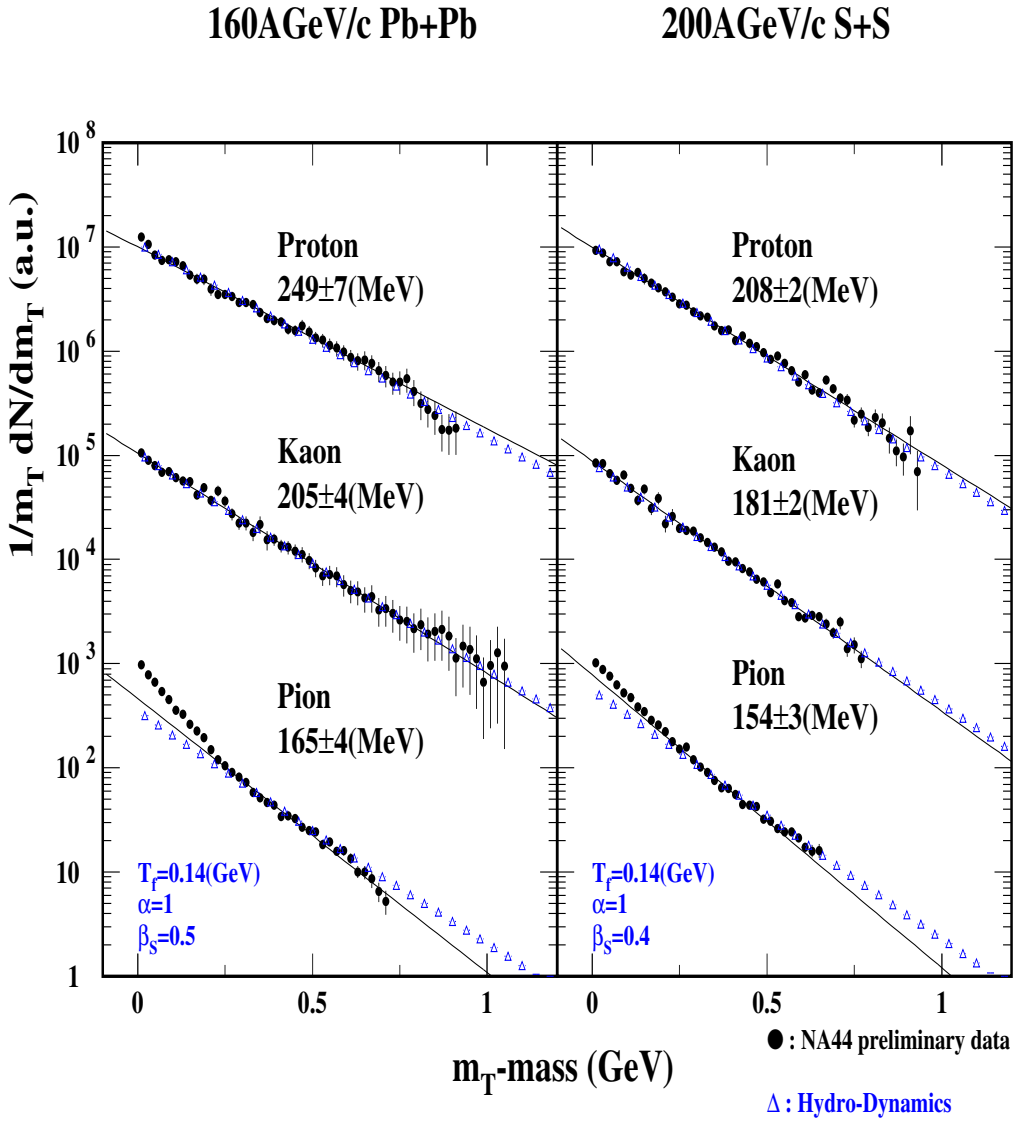

Figure 6-13: transverse mass spectra at T_f=140 MeV

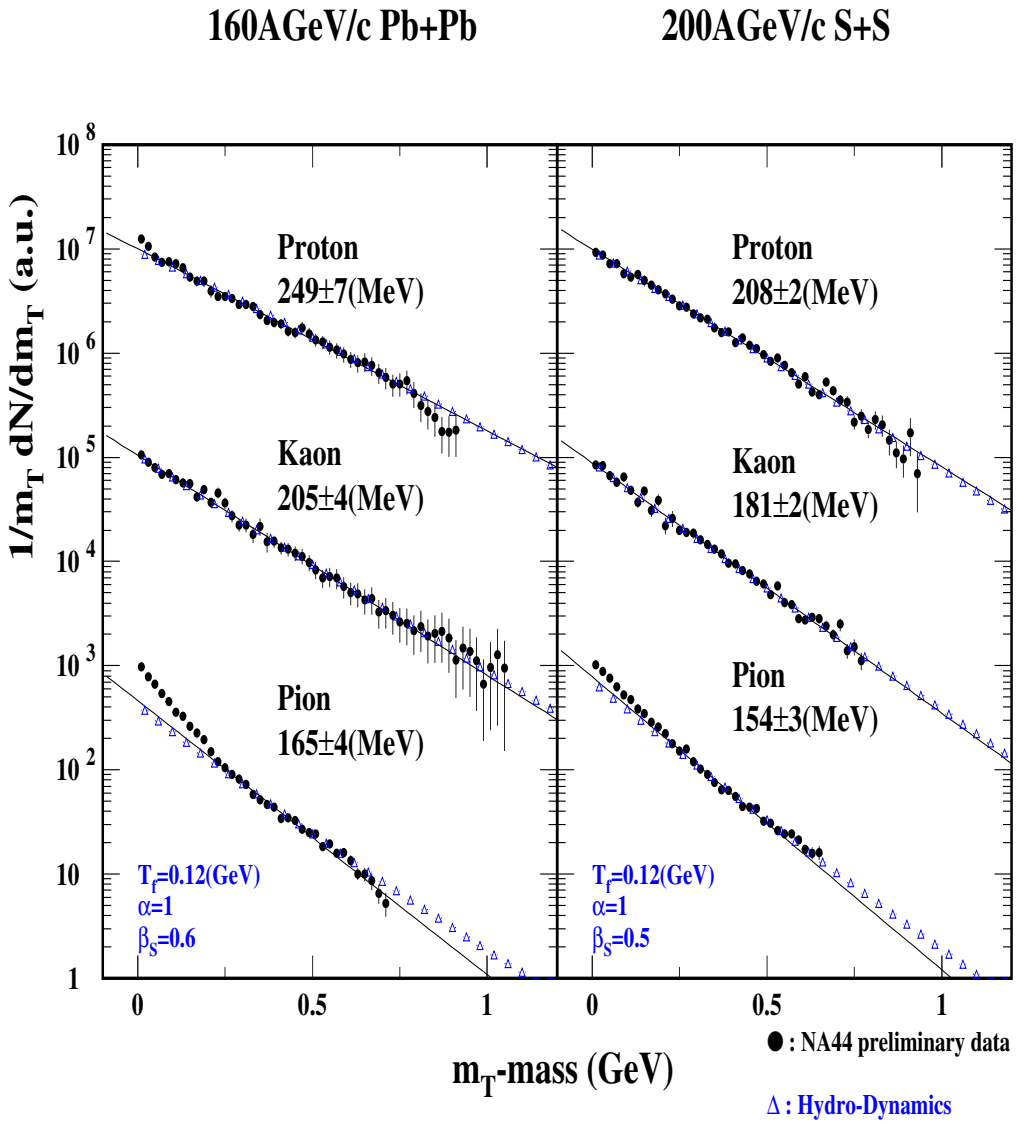

Figure 6-14: transverse mass spectra at T_f=120 MeV

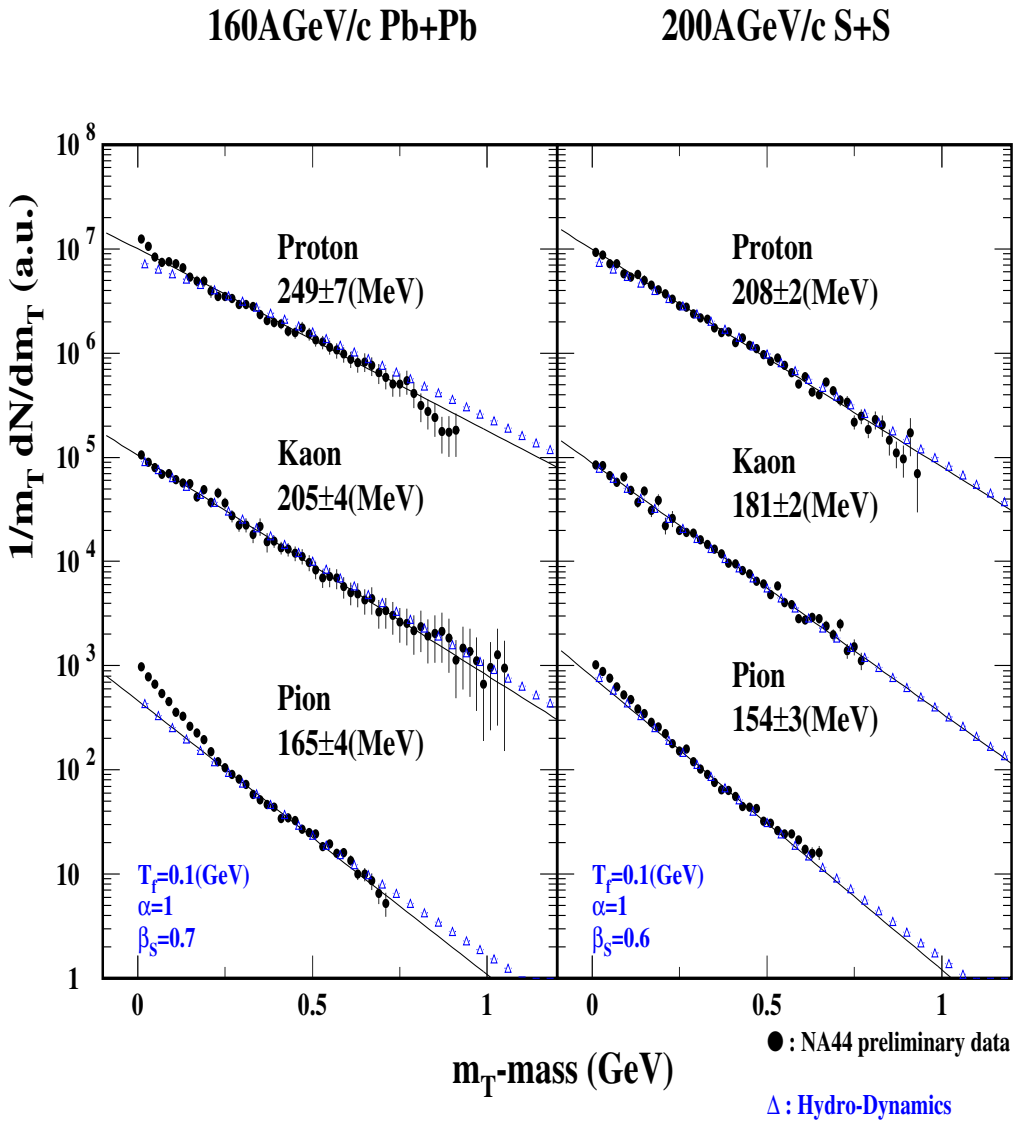

Figure 6-15: transverse mass spectra at T_f=100 MeV

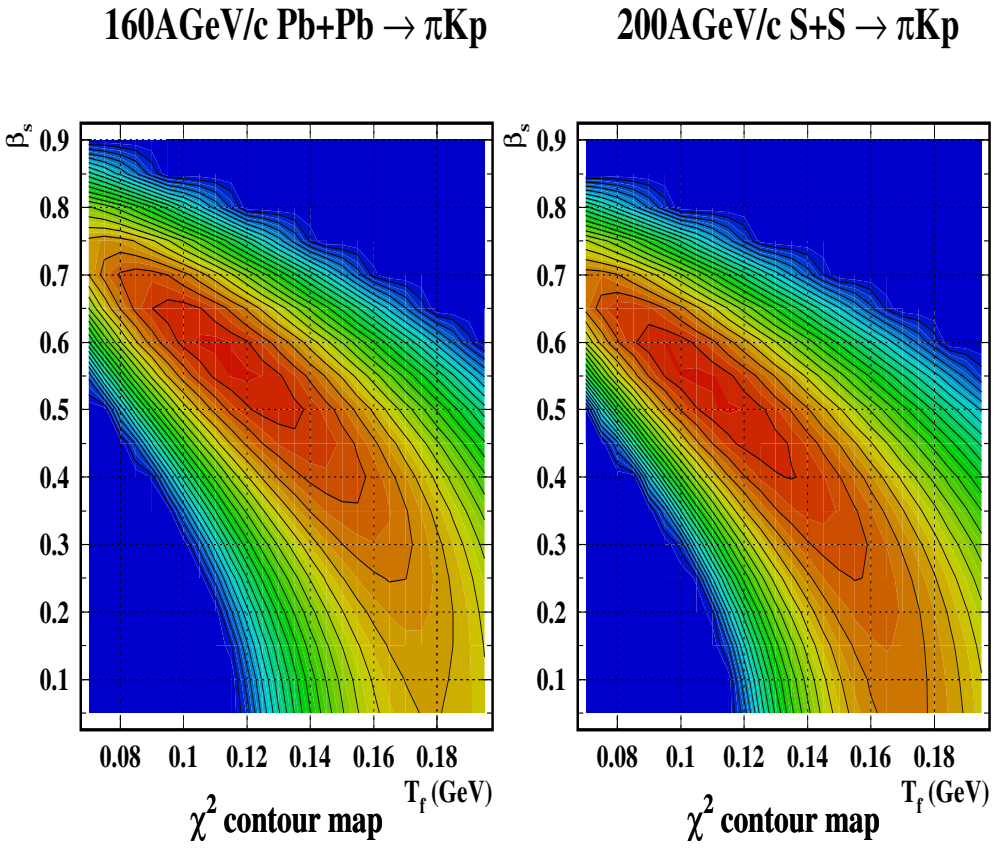

Figure 6-16: chi-square contour map over T_f and β_s

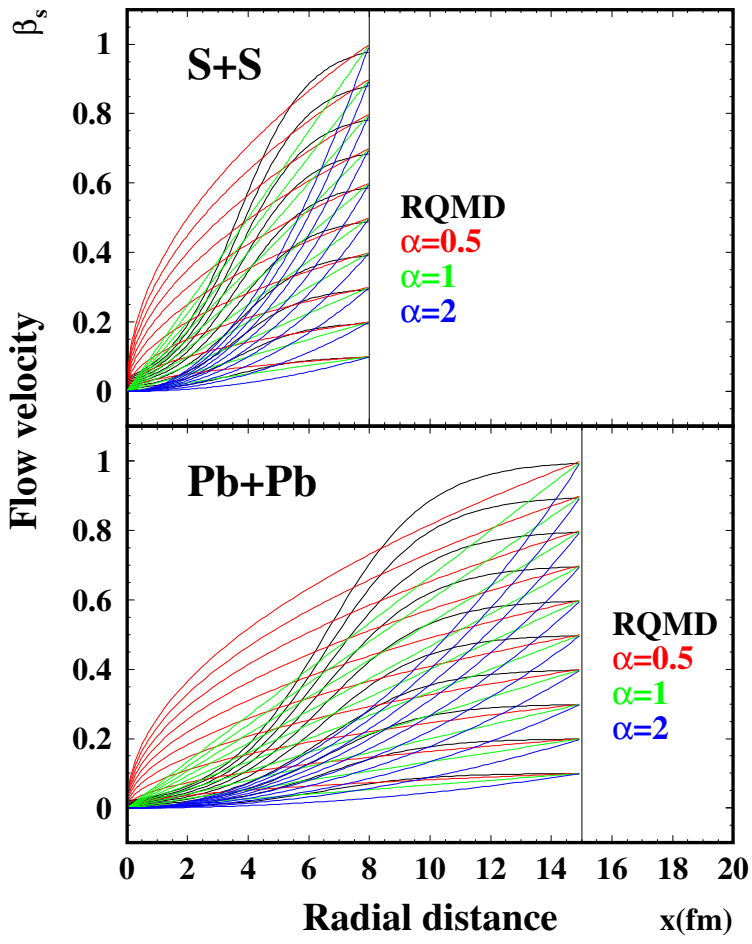

Figure 6-17: velocity profile

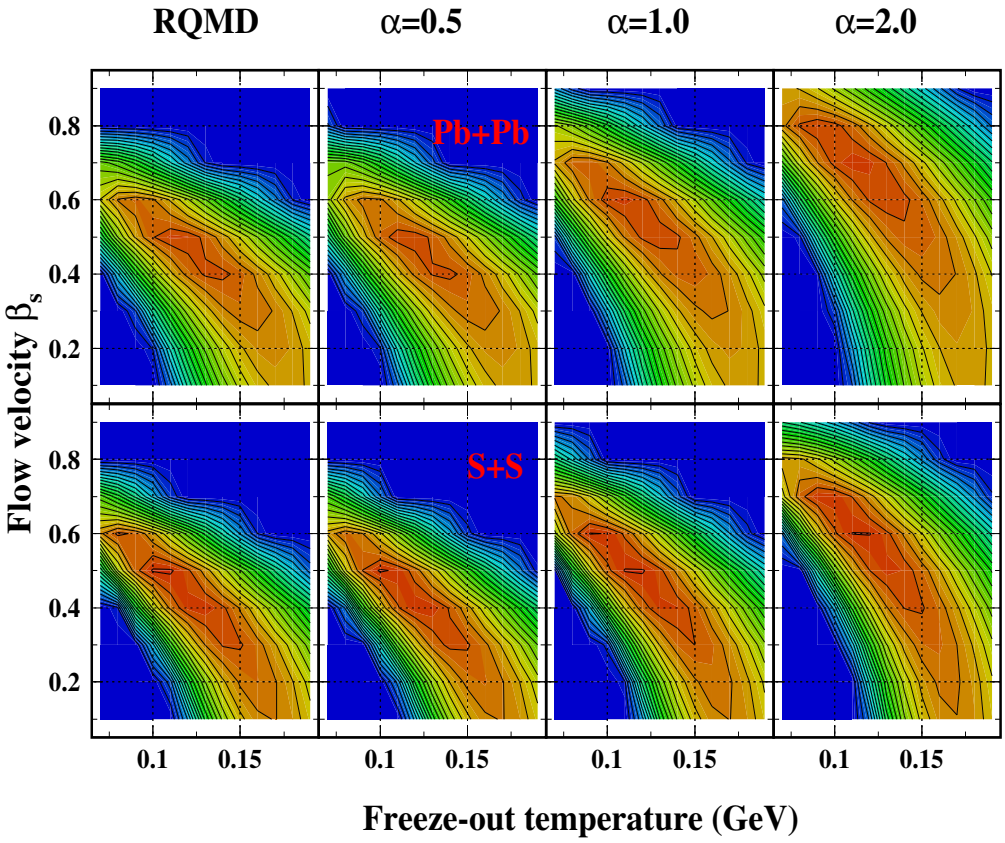

Figure 6-18: velocity profile dependence of chi-square map